separations

MDPI

Article

New Insights into the Mechanism of Gangue Contamination in Coking Coal Flotation: Roles of Water Entrainment and Slime Coating

Yunfei Zhang [1,2,3], Qi Zhang [2], Lijun Deng [4], Yijun Cao [1,2,3,5], Junchao Wang [1,2,3,5,*] and Guosheng Li [1,2,3,5,*]

1 State Key Laboratory of Critical Metal Benefication, Metallurgy and Purification, Zhengzhou University, Zhengzhou 450001, China; 15103867633@163.com (Y.Z.); caoyj@cumt.edu.cn (Y.C.)
2 School of Chemical Engineering, Zhengzhou University, Zhengzhou 450001, China; 15713855264@163.com
3 Luoyang Industrial Technology Institute, Zhengzhou University, Luoyang 450001, China
4 Center of Advanced Analysis & Gene Sequencing, Zhengzhou University, Zhengzhou 450001, China; okdenglijun@126.com
5 The Key Laboratory of Critical Metals Minerals Supernormal Enrichment and Extraction, Ministry of Education, Zhengzhou 450001, China
* Correspondence: wjccumt@163.com (J.W.); lgscumt@163.com (G.L.)

Abstract

Fine gangue contamination limits the flotation upgrading of coking coal middlings, yet the relative roles of water entrainment and slime coating remain unclear for different gangue minerals. This study investigated the contamination behaviors of quartz, kaolinite, and calcite through flotation tests, bubble-particle attachment measurements, zeta potential analysis, DLVO calculations, SEM-EDS observations, foam drainage and settling tests. Results showed that the addition of gangue minerals reduced combustible recovery, and the combustible recovery decreased from 91.68% for low-ash coal to 86.87%, 84.77%, and 82.55% for the coal–quartz, coal–kaolinite, and coal–calcite systems, respectively. Quartz exhibited limited coal–gangue association and a stronger tendency toward water entrainment, whereas calcite showed more pronounced surface attachment, consistent with slime-coating contamination. Kaolinite displayed intermediate behavior, with particle association that could not be fully explained by classical DLVO calculations. These findings demonstrated that gangue contamination depended on the combined effects of interfacial interactions, particle association, and water-mediated transport. The integrated approach provides a basis for identifying mineral-specific contamination tendencies and developing targeted strategies to improve flotation selectivity.

Keywords: coking coal flotation; gangue minerals; slime coating; water entrainment; contamination mechanism

Check for updates

Academic Editor: Qicheng Feng

Received: 8 October 2026
Revised: 26 October 2026
Accepted: 30 October 2026
Published: 5 November 2026

Copyright: © 2026 by the authors. Licensee MDPI, Basel, Switzerland. This article is an open access article distributed under the terms and conditions of the Creative Commons Attribution (CC BY) license.

1. Introduction

With the progressive depletion of easily exploitable high-quality coking coal resources, improving the recovery and utilization efficiency of existing coking coal reserves has become an important issue for the sustainable development of the coal industry [1,2]. Coking coal middlings still contain a considerable amount of combustible matter that can potentially be recovered through further beneficiation; however, they are frequently used as low-value fuels because of their complex mineral association and relatively poor separation response [3,4]. Improving the separation efficiency of coking coal middlings provides an effective way to enhance the recovery of valuable combustible components and increase

the overall resource utilization rate [5,6]. Nevertheless, the further upgrading of coking coal middlings remains challenging because of incomplete liberation, complex coal–gangue association, and the poor selectivity commonly encountered in fine-particle flotation [7–10].

Due to its ability to selectively recover hydrophobic coal particles from finely disseminated mineral matter, flotation has become an indispensable technique for upgrading coking coal middlings and improving resource recovery efficiency [11,12]. However, the liberation of coking coal middlings is inevitably accompanied by the generation of large amounts of fine coal and gangue particles [13,14]. On the one hand, fine gangue particles may be non-selectively transported into the froth concentrate with water, resulting in water entrainment. This process is strongly related to water recovery, froth drainage, particle size, hydrodynamic conditions, and froth properties [15–17]. On the other hand, fine gangue slimes can attach to coal surfaces and form slime coatings, which mask hydrophobic sites, reduce bubble-particle attachment probability, and consequently decrease combustible recovery [18–23]. Because water entrainment and slime coating may occur simultaneously in the same flotation system, conventional flotation indicators such as yield, ash content, and combustible recovery alone are often insufficient to identify the dominant contamination pathway. Distinguishing the relative importance of water-borne transport and direct surface association is therefore a key issue in understanding gangue contamination during coking coal middlings flotation.

Previous studies have greatly improved the understanding of slime coating and entrainment in fine-particle flotation. For example, Chen et al. [24] used zeta potential measurements and DLVO calculations to demonstrate that fine quartz and kaolinite could interact with coal particles and reduce bubble-particle attachment. Xing et al. [25] showed that different clay minerals exerted distinct effects on coal floatability through induction time and bubble-particle attachment measurements. Zhu et al. [26] investigated the mitigation of slime coating by inorganic regulators using flotation tests, SEM-EDS and interaction energy calculations. Yu et al. [19] revealed different coating tendencies of montmorillonite and kaolinite on coal surfaces using AFM measurements, while Li et al. [27] quantitatively characterized slime coating on coal surfaces by in situ PVM technology. In parallel, entrainment studies have shown that the recovery of fine gangue particles can be governed by water transport, and that froth drainage, water recovery and particle properties are critical factors affecting entrainment behavior [28–31].

These studies provide important foundations for understanding gangue contamination in flotation. However, many of them considered slime coating or water entrainment separately, whereas their relative contributions are difficult to distinguish when both pathways operate simultaneously in the same flotation system. In addition, zeta potential measurements and classical DLVO calculations mainly describe averaged electrokinetic properties and long-range interaction tendencies. For anisotropic minerals such as kaolinite, local edge-face interactions may differ from the averaged surface response; for reactive minerals such as calcite, aqueous dissolution and ion-mediated effects may also modify the interface. Thus, no single characterization method is sufficient to distinguish water-mediated transport from coal–gangue surface association. A complementary evidence chain combining flotation response, bubble-particle attachment, interfacial interaction analysis, direct surface observation, suspension stability, and foam drainage characterization is therefore required.

In this study, quartz, kaolinite, and calcite were selected as representative gangue minerals because they were identified among the major mineral phases in the coking coal middlings. The single-gangue mineral systems were designed as simplified model systems to decouple mineral-specific effects and are not intended to reproduce the quantitative flotation performance of an industrial feed containing multiple gangue minerals at different abundances and liberation states. In an industrial system, the contribution of each mineral

would additionally depend on its abundance, liberation degree, particle-size distribution, and occurrence mode. To address these issues, this study investigated the contamination behaviors of quartz, kaolinite, and calcite in simplified coking coal–gangue flotation systems. Flotation kinetics and water recovery measurements were combined with bubble-particle attachment tests, zeta potential analysis, DLVO calculations, SEM-EDS observations, foam drainage, and settling tests to distinguish the relative tendencies of water entrainment and slime coating. The objective was to clarify how mineral-specific interfacial interactions and particle association influence coal floatability and gangue recovery. By integrating these complementary measurements, this study provides a comparative mechanistic framework for understanding gangue contamination and offers insights into the selective control of fine gangue minerals during coking coal flotation.

2. Materials and Methods

2.1. Materials

The coal sample was collected from the Coal Preparation Plant of Shenma Pingmei Group, Pingdingshan City. Quartz was sourced from Wenshan City. Calcite was purchased from Guilin City. And kaolinite was obtained from Chenzhou City. The coal sample was air-dried, crushed, and ground to −74 μm for flotation tests. Quartz, kaolinite, and calcite were ground to −74 μm for subsequent tests. The mineralogical compositions of these samples were characterized by X-ray diffraction (XRD), and the diffraction patterns were presented in Figure 1.

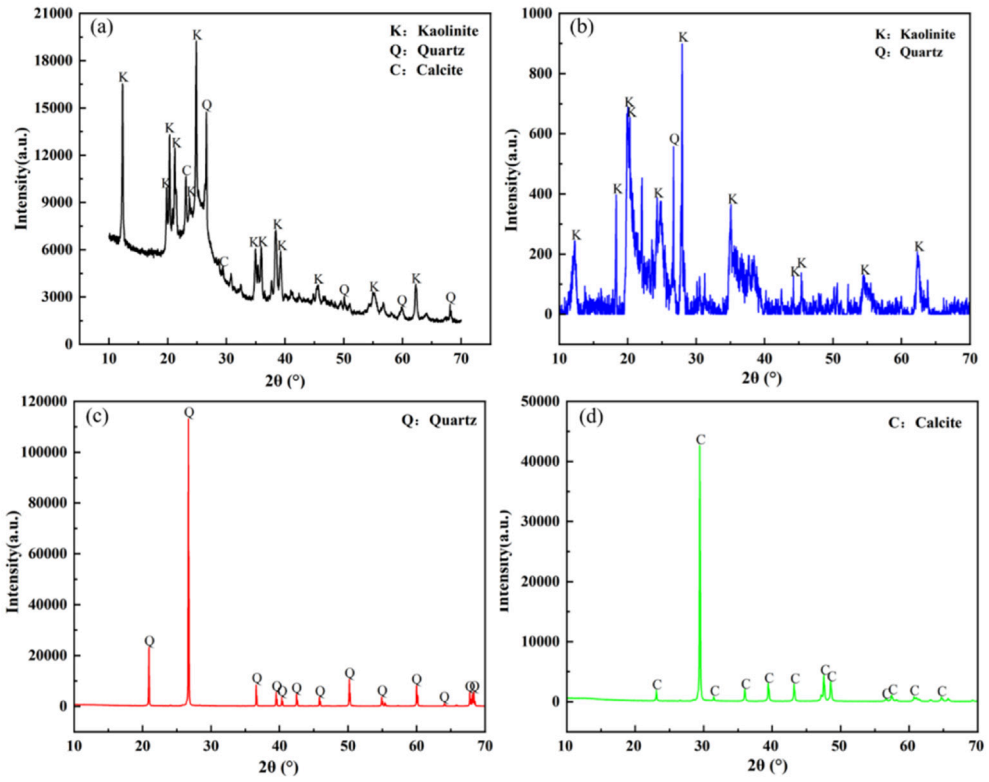


Figure 1. XRD patterns of the minerals: (**a**) coking coal middlings; (**b**) kaolinite; (**c**) quartz; (**d**) calcite.

As shown in Figure 1a, kaolinite exhibited the most prominent diffraction peaks among the identified mineral phases in the coal sample, whereas quartz and calcite were also detected. These results indicated that kaolinite, quartz, and calcite were the main crystalline gangue phases identified in the coal sample. Therefore, these minerals were selected as representative gangue minerals for subsequent contamination mechanism investigations. In

addition, the minor quartz impurity peaks were observed in the kaolinite sample (Figure 1b); however, kaolinite remained the predominant phase. Figure 1c,d indicated that the quartz and calcite samples had high-intensity diffraction peaks with few impurity peaks, suggesting relatively high phase purity.

The results of the proximate and ultimate analyses of the coal sample are presented in Tables 1 and 2, respectively. The proximate analysis showed an ash content of 24.23%, a moisture content of 0.29%, and a fixed carbon content of 55.50% on an air-dried basis. The ultimate analysis indicated that carbon was the predominant element among those analyzed, accounting for 63.53%, followed by oxygen (7.59%) and hydrogen (3.24%).

Table 1. Proximate analysis of the coal sample (ad: air-dried basis; d: dry basis).

Index	Moisture	Ash (%)		Volatile (%)			Fixed Carbon
	M_{ad} (%)	A_{ad}	A_d	V_{ad}	V_d	V_{daf}	F_{Cad} (%)
Value	0.29	24.23	24.30	19.98	20.04	26.47	55.50

Table 2. Ultimate analysis of the coal sample.

Index	C (%)	H (%)	N (%)	S (%)	O (%)
Value	63.53	3.24	0.99	0.19	7.59

Although no distinct crystalline carbon peaks were identified in the XRD pattern (Figure 1a), this does not contradict the carbon content determined by ultimate analysis, as the carbonaceous matter in coal generally exhibits a poorly ordered structure. Unlike XRD, which primarily identifies crystalline mineral phases, ultimate analysis characterizes the contents of selected elements, including C, H, N, S, and O. Therefore, mineral-associated elements such as Si, Al, and Ca are not included in Table 2, and the reported elemental contents should not be interpreted as a complete elemental mass balance of the coal sample. These results provide complementary information on the basic composition of the coking coal middlings.

2.2. Experimental Methods

The experimental program was designed to distinguish the contamination tendencies of quartz, kaolinite, and calcite in coking coal flotation through complementary measurements. Flotation kinetic tests were conducted to evaluate combustible recovery and the relationship between gangue recovery and water recovery. However, flotation results alone cannot distinguish water entrainment from slime coating, as both mechanisms may occur simultaneously.

To further investigate these mechanisms, induction time and bubble-particle attachment angle measurements were used to assess coal floatability, while zeta potential distributions and DLVO calculations characterized coal–gangue interfacial interactions. SEM-EDS and settling tests provided evidence of gangue attachment and particle aggregation, respectively, whereas foam drainage experiments evaluated water retention and drainage behavior. By integrating these measurements, the dominant contamination tendencies of different gangue minerals could be comparatively assessed, although the individual contributions of water entrainment and slime coating were not quantitatively separated.

2.2.1. Coking Coal Middlings Flotation Tests

Coking coal middlings flotation tests were conducted to evaluate the influence of grinding time and collector dosage on flotation performance. All tests were carried out in a

1.5 L XFG single-cell flotation machine (Wuhan Exploration Machinery Co., Ltd., Wuhan, China). The pulp concentration was maintained at 5 wt%, the impeller speed was fixed at 1900 rpm, and the airflow rate was controlled at 0.2 m^3/h. Kerosene and 2-octanol were used as the collector and frother, respectively. The grinding time was varied from 5 to 9 min, and the kerosene dosage was adjusted from 120 to 360 g/t. The 2-octanol dosage was fixed at 70 g/t. For each test, the coal sample was added to the flotation cell and conditioned for 2 min. Subsequently, kerosene was added and conditioned for 2 min, followed by the addition of 2-octanol with a further conditioning period of 1 min. Air was then introduced into the flotation cell, and flotation was conducted for 3 min after 10 s of aeration. The flotation products were filtered, dried, weighed, and subjected to ash analysis. The clean coal yield was calculated from the mass ratio of the concentrate to the feed. Note that each test was repeated three times, and the average values were presented.

2.2.2. Low-Ash Coal–Gangue Mixed System Flotation Tests

A separate low-ash coking coal with an ash content of approximately 5% was selected as the model coal for the mechanistic tests. Flotation tests of low-ash coal and gangue mixed systems were conducted using a 1.5 L XFG single-cell flotation machine. The pulp concentration was maintained at 5%, and the impeller speed was set to 1900 rpm. Kerosene and 2-octanol were used as the collector and frother, respectively. For the binary systems, low-ash coal and gangue minerals were mixed at a coal-to-gangue mass ratio of 1:1. The coal sample or coal–gangue mixture was first added to the flotation cell and conditioned for 2 min. Kerosene and 2-octanol were subsequently added, with conditioning times of 2 min and 1 min, respectively. Aeration was then initiated, and flotation was performed after 10 s of air introduction. Concentrate products were collected at 0.5, 1.5, 2.5, 3.5, and 4.5 min to obtain time-resolved flotation recovery data and evaluate the flotation kinetics of the low-ash coal and coal–gangue mixed systems. The collected froth products were transferred to pre-weighed glass dishes, weighed, filtered, dried, and analyzed for ash content. Flotation performance is evaluated in terms of combustible recovery (C_R), apparent gangue recovery (G_R), and water recovery (R_w), which are calculated using Equations (1)–(4) [32,33].

$$C_R = \frac{M_c(100 - A_c)}{M_f(100 - A_f)} \times 100 \quad (1)$$

$$G_R = \frac{M_c A_c}{M_f A_f} \times 100 \quad (2)$$

$$R_w = \frac{W_c}{W_f} \times 100 \quad (3)$$

The time-dependent combustible recovery data were fitted using a first-order flotation kinetic model:

$$R_t = R_\infty(1 - e^{-kt}) \quad (4)$$

where M_c is the mass of concentrate (g); M_f is the mass of feed (g); A_c is the ash content of concentrate (%); A_f is the ash content of feed (%); W_c is the mass of water recovered in the concentrate (g); and W_f is the total mass of water in the flotation pulp (g), where Rt is the combustible recovery at flotation time t, R_∞ is the ultimate combustible recovery, and k is the flotation rate constant. The fitting parameters were used to compare the flotation-rate differences among different coal–gangue systems.

2.2.3. Induction Time and Bubble-Particle Attachment Angle (BPAA) Measurements

Induction time was defined as the minimum bubble-particle contact time corresponding to a 50% attachment probability, following the established criterion used in bubble-particle attachment measurements [25]. A smaller induction time indicates a higher probability of bubble-particle attachment under otherwise identical conditions. Unlike the

flotation experiments, the induction time measurements were conducted using a separate laboratory-scale bubble-particle attachment apparatus, as schematically illustrated in Figure 2a. The self-designed apparatus consisted of a transducer, a measurement cell, a microsyringe, a high-speed camera, and a light source. A single air bubble with a diameter of 3.0 ± 0.1 mm was generated at the tip of a capillary connected to the microsyringe. The bubble was initially positioned 2 mm above a coal particle bed consisting of 2 g of coal particles with a size range of 0.25–0.5 mm. During each measurement, the bubble approached the particle bed at a controlled velocity of 20 mm/s and remained in contact with the particles for a predetermined duration before being withdrawn. The attachment or detachment of coal particles was recorded using the high-speed camera. The induction time was determined from 20 independent trials per condition based on the contact duration corresponding to a 50% attachment probability.

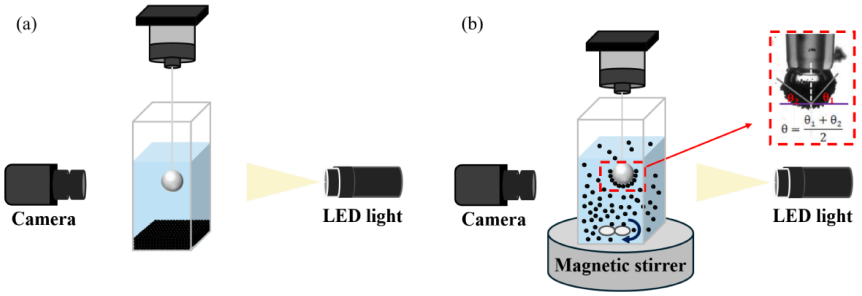


Figure 2. Schematic illustrations of the experimental setups: (**a**) induction time measurements and (**b**) BPAA measurements.

To evaluate slime coating effects, low-ash coal particles were pre-conditioned with quartz, kaolinite, or calcite (coal/gangue = 5:1) in 200 mL deionized water at 1000 rpm for 4 min, followed by 1 min settling [25]. BPAA measurements were used as the complementary indicator of floatability, defined as the angular coverage of particles on the bubble surface. Coal particles (0.125~0.25 mm) were conditioned with gangue minerals under the same protocol and analyzed in a stirred cell at 250 rpm. Bubble images were captured at 30~150 s, and BPAA was quantified using ImageJ 2 software. All tests were conducted in triplicate. The experimental setups used for induction time and BPAA measurements are schematically illustrated in Figure 2.

2.2.4. Zeta Potential Distribution Tests

Zeta potential distribution tests of low-ash coal, quartz, kaolinite, calcite, and their binary mixtures were conducted using a zeta potential analyzer (ZSE, Malvern, UK). Suspensions were prepared by dispersing 1 g of sample in 1 L of 0.1 mM NaCl solution and stirring for 5 min. For the binary systems, low-ash coal and gangue minerals were mixed at a coal-to-gangue mass ratio of 2:1 and subjected to the same preparation procedure. All measurements were performed at the natural pH of the suspensions without further pH adjustment, in order to reflect the interfacial behavior under the original suspension conditions. The natural pH values of the binary coal–gangue suspensions were measured before zeta potential analysis. The measured pH values were 7.88 for the coal–quartz system, 6.91 for the coal–kaolinite system, and 7.86 for the coal–calcite system, indicating that the interfacial measurements were conducted under near-neutral to weakly alkaline conditions. After standing for 5 min to allow coarse particles to settle, 1 mL of the supernatant was collected and transferred into a disposable capillary cell for analysis. The zeta potential distributions and average zeta potentials were obtained from three independent measurements. The measured zeta potentials were used as apparent surface potentials for the subsequent

DLVO calculations. Accordingly, the zeta-potential and DLVO results should be interpreted specifically within the near-neutral to weakly alkaline pH range investigated here rather than generalized to all flotation pH conditions.

It should be noted that the present measurements were intended to characterize the zeta potential distributions of individual minerals and their binary mixtures under natural pH conditions, rather than to determine their isoelectric points (IEPs). The IEP is defined as the pH at which the zeta potential reaches zero and generally requires measurements over a range of pH values. Since no systematic pH adjustment was performed in this study, the IEPs of the investigated minerals were not determined.

2.2.5. DLVO Theoretical Analysis

The interaction tendency between low-ash coal and gangue particles was evaluated using DLVO theory, in which the total interaction energy (E_{total}) was expressed as the sum of van der Waals attraction (E_{vdw}) and electrostatic double-layer interaction energy (E_{edl}). The van der Waals interaction energy between two spherical particles can be expressed as Equation (5) [34]:

$$E_{vdw} = -\frac{A_{132}}{6h}\frac{R_1 R_2}{R_1 + R_2} \tag{5}$$

The effective Hamaker constant (A_{132}) for the coal–water–gangue system was calculated using Equation (6):

$$A_{132} = \frac{3k_B T}{4} + \frac{3h_1\omega}{8\sqrt{2}} \times \frac{(n_1^2 - n_3^2)(n_2^2 - n_3^2)}{(n_1^2 + n_3^2)\sqrt{n_2^2 + n_3^2} + (n_2^2 + n_3^2)\sqrt{n_1^2 + n_3^2}} \tag{6}$$

The electrostatic double-layer interaction energy can be calculated using Equation (7) [35]:

$$E_{edl} = \frac{\varepsilon\varepsilon_0\pi R_1 R_2}{R_1 + R_2}\left[2\psi_1\psi_2 \ln\frac{1 + e^{-\kappa h}}{1 - e^{-\kappa h}} + (\psi_1^2 + \psi_2^2)\ln(1 - e^{-2\kappa h})\right] \tag{7}$$

where A_{132} is the Hamaker constant, R_1 and R_2 are the radii of coal and gangue particles, h is the distance between particles, K_B is the Boltzmann constant (1.381×10^{-23} J/K), T is temperature (293.15 K in this experiment), h_1 is Planck's constant (6.626×10^{-34} J·s), ω is the characteristic relaxation frequency in the UV region (2.068×10^{16} rad/s). n_1, n_2, n_3 are the refractive indices of coal, gangue, and water (coal: 1.70; quartz: 1.544; kaolinite: 1.553; calcite: 1.50; water: 1.33). ε is the relative permittivity of 0.1 mmol/L NaCl solution (78.5 C^2·m/J). ε_0 is the vacuum permittivity (8.854×10^{-12} C^2·m/J). ψ_1 and ψ_2 represent the surface potentials of coal and gangue particles and are approximated using the measured zeta potentials. κ^{-1} is the Debye length (30.4 nm in 0.1 mmol/L NaCl solution). The Hamaker constants were not experimentally measured in this study; the effective constants were calculated from the Lifshitz-type relation using the refractive indices of coal, the gangue mineral, and water given above. They therefore represent calculated effective constants rather than experimentally measured surface-specific values.

It should be noted that the classical DLVO model was used here as a first-order comparative approach to evaluate the relative long-range interaction tendencies between coal and different gangue minerals. This model assumes spherical particles and considers only van der Waals and electrostatic double-layer interactions. Therefore, it does not explicitly account for the platy morphology and facet-dependent surface charge heterogeneity of kaolinite, nor does it include hydration interactions, acid-base interactions, hydrophobic interactions, or dissolution-related aqueous chemistry of calcite. These limitations were considered when interpreting the DLVO results, and the calculated interaction energy profiles were used to assess the relative tendency toward coal–gangue heteroaggregation rather than to provide an absolute prediction of slime coating behavior.

2.2.6. SEM-EDS Measurements

SEM-EDS was employed to characterize the surface morphology and elemental composition of low-ash coal particles before and after conditioning with gangue minerals. A Sigma 300 scanning electron microscope (Carl Zeiss Group, Oberkochen, Germany) equipped with an EDS detector was operated at an accelerating voltage of 15 kV. A mixture containing 5 g of low-ash coal and 1 g of gangue mineral was dispersed in 500 mL of 0.1 mM NaCl solution and conditioned at 500 rpm for 10 min. The suspension was subsequently filtered, and the collected solids were dried at room temperature. Prior to SEM observation, the dried samples were sputter-coated with gold to improve conductivity. SEM images were obtained from representative regions of coal particles to examine the changes in surface morphology after conditioning with different gangue minerals. EDS point analysis was conducted on selected attached particles or surface regions to identify their characteristic elemental signatures. Si and O were used as the characteristic elements for quartz, Si, Al, and O for kaolinite, and Ca and O for calcite. The SEM-EDS results were used to verify the presence of gangue particles on coal surfaces and to support the interpretation of coal–gangue surface association and slime coating behavior together with the zeta potential, DLVO, and bubble-particle attachment results.

2.2.7. Foam Drainage Tests

Foam drainage tests were conducted using a self-designed drainage apparatus to estimate the contribution of water entrainment to gangue recovery. A 1.5 L XFG flotation cell was employed as the froth generation device, with an aeration rate of 0.2 m^3/h, an impeller speed of 1900 rpm, and a pulp concentration of 5 wt%. To investigate the influence of gangue minerals on froth drainage behavior, quartz, kaolinite, and calcite were individually mixed with low-ash coal at gangue proportions of 0%, 20%, 40%, 60%, and 80%, while maintaining a constant total solid mass of 75 g. The gangue proportion refers to the mass percentage of gangue mineral in the total solids. The mixed samples were conditioned for 2 min prior to reagent addition. Kerosene (120 g/t) was then added as the collector and conditioned for a further 120 s, followed by the addition of 2-octanol (70 g/t) as the frother and conditioning for 1 min.

Subsequently, air was introduced into the flotation cell. After 10 s of aeration, the generated froth was rapidly transferred into the drainage tube shown in Figure 3. Approximately 500 mL of froth was collected for each test. The drainage valve was opened immediately after froth collection, and the froth was allowed to drain for 8 min. After drainage, the drained liquid and residual froth were collected separately. The masses of the drained liquid and residual froth were recorded. Both fractions were then filtered, dried, weighed, and analyzed for solid mass and ash content. All measurements were conducted in triplicate, and the average values were reported. The contribution of water entrainment (C_{we}) to gangue recovery is calculated according to Equation (8) [36]:

$$C_{we} = \frac{100 M_{ws} \cdot A_{ws}}{(M_{fs} \cdot A_{fs} + M_{ws} \cdot A_{ws})} \quad (8)$$

where M_{fs} is the solid mass recovered in the residual froth after drainage (g); M_{ws} is the solid mass in drained liquid regarded as the apparent gangue fraction transported by the water phase (g); A_{fs} is the ash content of solids recovered in the residual froth (%); A_{ws} is the ash content of solids in percolated liquid (%).

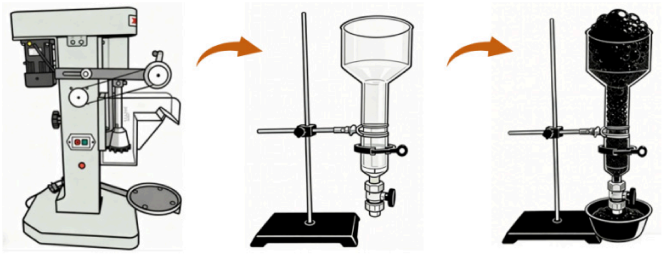


Figure 3. Schematic of foam drainage test process and apparatus.

2.2.8. Settling Tests

Settling tests were performed using a 100 mL graduated glass cylinder to evaluate the sedimentation behavior of low-ash coal, quartz, kaolinite, calcite, and their binary mixtures. For the single-component systems, 1.5 g of low-ash coal or an individual gangue mineral was dispersed in deionized water and diluted to a final volume of 100 mL. The coal-to-gangue mass ratio in the binary systems was maintained at 2:1, then they were added simultaneously, and the suspension volume was adjusted to 100 mL with deionized water. The graduated cylinder was inverted 20 times to disperse the particles uniformly and then left undisturbed for quiescent settling. Digital photographs were taken at 0, 5, 10, 15, and 20 min. The clarified liquid height was defined as $Hc(t)$, measured from the liquid surface to the suspension interface at settling time t. For a cylinder with initial liquid height H0 and suspension-interface height $Hi(t)$ measured from the cylinder bottom, $Hc(t)$ was defined as $Hc(t) = H0 - Hi(t)$. No additional normalization was applied. A larger $Hc(t)$ indicates faster apparent particle settling and a clearer supernatant, whereas a smaller $Hc(t)$ indicates that more particles remained dispersed. The single-component and binary systems were compared to provide macroscopic evidence consistent with different coal–gangue heteroaggregation tendencies.

3. Results

3.1. Flotation Test Results

3.1.1. Results of Coking Coal Middlings Flotation Tests

Coking coal middlings flotation tests were conducted to investigate the effects of grinding time and collector dosage on flotation performance. The yield and ash content of clean coal were measured to determine the optimal flotation conditions. And the variations in the yield and ash content of clean coal with grinding time under different collector dosages are shown in Figure 4.

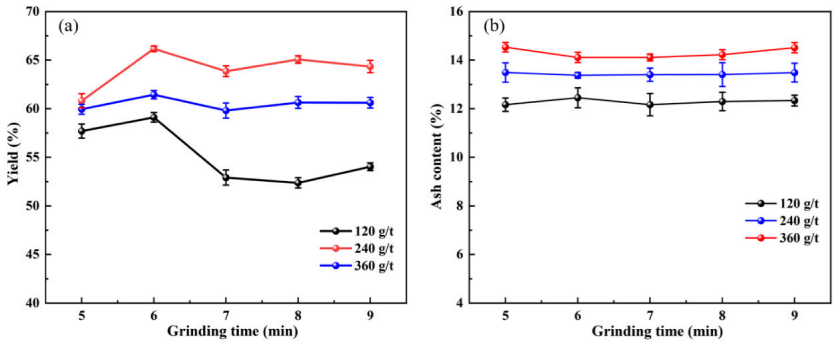


Figure 4. Coking coal middlings flotation test results under different grinding times and collector dosages (**a**) yield; (**b**) ach content.

As shown in Figure 4a, the clean coal yield initially increased when the grinding time was increased from 5 to 6 min. This indicates that moderate grinding promoted the liberation of combustible components from associated gangue minerals and improved the recovery of floatable coal particles. However, further increasing the grinding time did not lead to a continuous increase in clean coal yield. This phenomenon may be related to the generation of additional fine particles during excessive grinding, which can deteriorate flotation selectivity and reduce the effective recovery of clean coal. Meanwhile, increasing the kerosene dosage from 120 to 360 g/t increased the clean coal yield from 58.77% to 66.37%, suggesting that a higher collector dosage promoted the recovery of hydrophobic coal particles.

However, the increase in clean coal yield was accompanied by a deterioration in product quality. As shown in Figure 4b, the ash content of clean coal increased from approximately 12% at 120 g/t kerosene to more than 14% at higher collector dosages. This yield-ash trade-off indicates that the recovery of combustible matter was accompanied by the simultaneous recovery of fine gangue particles. Therefore, simply increasing the collector dosage improved coal recovery but reduced flotation selectivity.

Based on the balance between clean coal yield and ash content, a grinding time of 6 min and a kerosene dosage of 120 g/t were selected as the baseline conditions for the following experiments. The flotation results of the original coking coal middlings provide a practical reference for the overall separation response of the complex feed. However, because the original sample contains multiple gangue minerals with different proportions, liberation states, and associations, conventional flotation indicators alone cannot quantitatively distinguish the individual contributions of different gangue minerals or determine whether a given mineral is recovered mainly by water entrainment or slime coating. Therefore, the simplified low-ash coal–gangue model systems were used to isolate mineral-specific behaviors. The results from these model systems should consequently be interpreted as mechanistic descriptors that can help explain possible contamination pathways in the original feed, rather than as additive predictions of its mineral-specific flotation recovery.

3.1.2. Results of Coal–Gangue Mixed System Flotation Tests

To clarify the contamination behaviors of different gangue minerals during coking coal flotation, flotation kinetics and the relationship between gangue recovery and water recovery were investigated for low-ash coal and the corresponding coal–gangue mixtures, as shown in Figure 5. The time-resolved kinetic curves characterize the flotation-rate responses of the simplified systems, whereas the gangue-recovery/water-recovery relationship provides a first indication of whether gangue recovery is closely associated with hydraulic water transport.

As shown in Figure 5a, the addition of gangue minerals decreased the combustible recovery of clean coal. The final recovery at 270 s declined from 91.68% for low-ash coal to 86.87%, 84.77%, and 82.55% for the coal–quartz, coal–kaolinite, and coal–calcite systems, respectively, indicating that gangue contamination progressively deteriorated flotation performance [37,38]. The depression effect followed the order of calcite > kaolinite > quartz, indicating that different gangue minerals affected coal flotation to different extents under the same operating conditions. Additionally, it could be seen from Figure 5b that gangue recovery in the coal–quartz system increased almost linearly with water recovery, indicating that quartz recovery was predominantly governed by water entrainment. In contrast, the coal–calcite system exhibited a rapid increase in gangue recovery at low water recovery, followed by a plateau, suggesting that mechanisms other than water entrainment dominated its recovery [39]. The coal–kaolinite system exhibited an intermediate behavior. Therefore, the flotation results provided preliminary evidence for mineral-dependent contamination

tendencies, which were further examined by the subsequent interfacial interaction, foam drainage, SEM-EDS, and settling analyses.

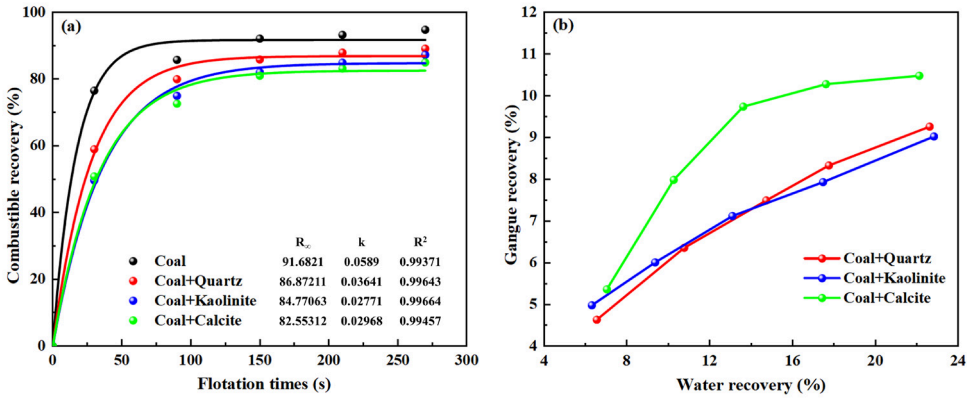


Figure 5. Flotation performance of low-ash coal mixed with different gangue minerals: (**a**) flotation kinetics; (**b**) relationship between water recovery and gangue recovery.

3.2. Results of BPAA and Induction Time Measurements

To investigate the influence of different gangue minerals on bubble-particle attachment, the induction time and BPAA were measured for the coal–gangue mixed systems. The results are presented in Figure 6.

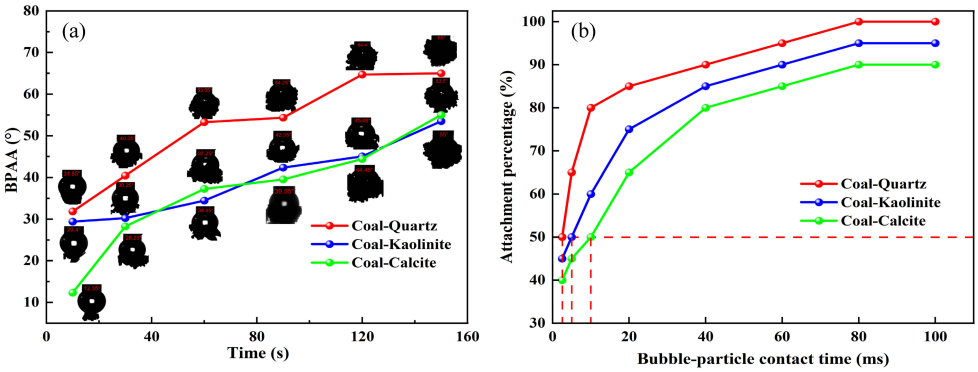


Figure 6. BPAA and induction time measurement results of the coal–gangue mixed systems: (**a**) BPAA; (**b**) induction time. The red line represents the induction time value for each substance.

As shown in Figure 6a, the BPAA increased with flotation time and gradually reached a stable value for all coal–gangue mixed systems. The coal–quartz system exhibited the largest BPAA (approximately 65°), followed by the coal–kaolinite and coal–calcite systems (approximately 55°), indicating that quartz had the least influence on the bubble-coal attachment capacity. The induction time also showed a corresponding trend of change (Figure 6b): the red line represents the induction time value for each substance. The induction time of the coal–quartz system was 2.5 ms, while the induction times of the coal–kaolinite system and the coal–calcite system were 5 ms and 10 ms, respectively. The prolonged induction time indicated a lower probability of bubble-particle attachment, demonstrating that calcite exerted the strongest inhibition on coal floatability, followed by kaolinite and quartz. These results were consistent with the flotation kinetics (Figure 5), which showed the same relative inhibition tendency of calcite > kaolinite > quartz. The contrasting attachment behaviors suggested that the three gangue minerals interacted differently with coal surfaces, which was further examined through interfacial interaction analyses. The different attachment responses suggest that the three gangue minerals altered

coal surface properties or coal–gangue association to different extents, which was further examined using zeta potential distribution, DLVO calculation, SEM-EDS, foam drainage, and settling analyses.

3.3. Results of Zeta Potential Distribution Tests

To investigate the electrokinetic characteristics and interfacial association behavior of low-ash coal and gangue minerals, zeta potential distributions were measured under the natural pH conditions of the corresponding suspensions, as shown in Figure 7. The peak positions in these distributions represent the characteristic zeta potentials of the measured particle populations rather than their isoelectric points. As shown in Figure 7a,b, low-ash coal and quartz exhibited unimodal zeta potential distributions with peaks at −20.59 mV and −41.15 mV, respectively. After mixing, the coal–quartz suspension retained a bimodal distribution with peak positions close to those of the individual components, suggesting that the two particle populations largely maintained their distinct electrokinetic characteristics and exhibited relatively limited interfacial association [40].

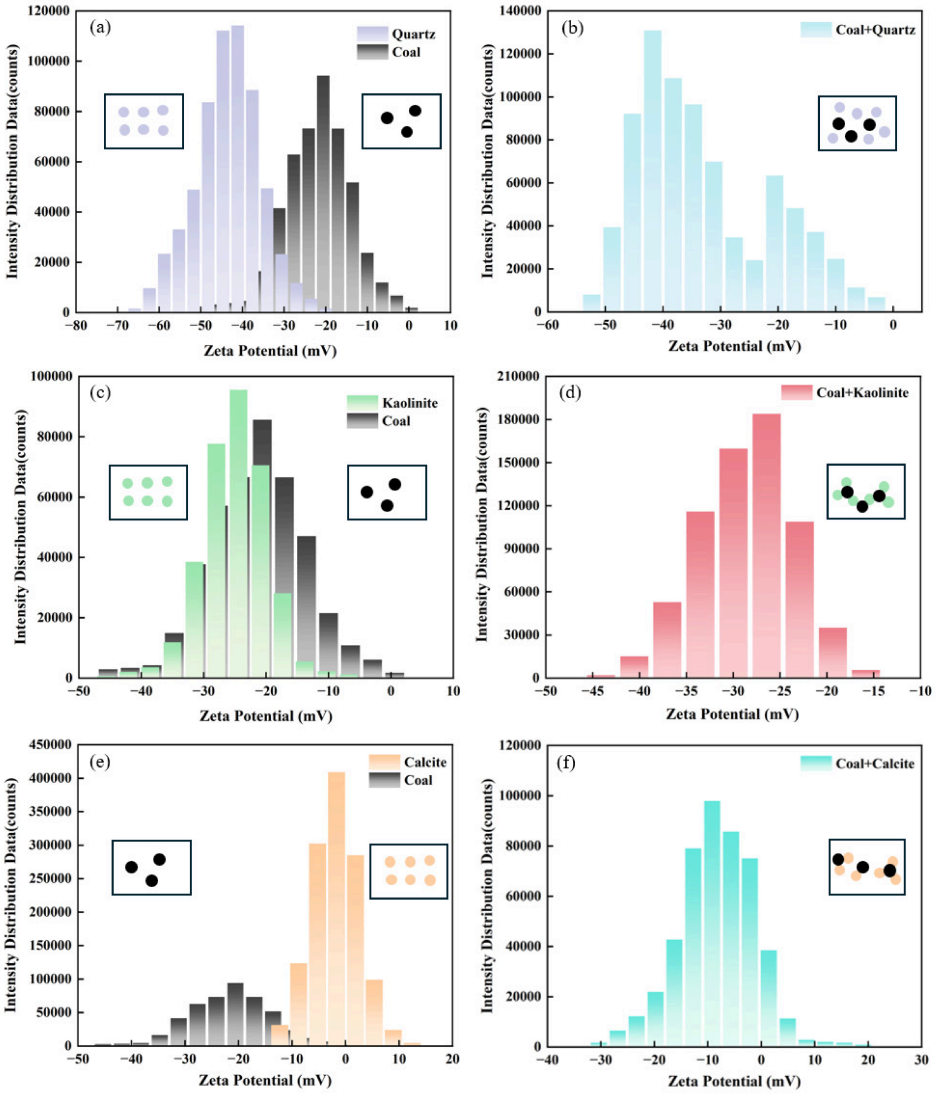


Figure 7. Zeta potential distributions of low-ash coal, gangue minerals, and their mixtures: (**a**) coal and quartz; (**b**) coal–quartz system; (**c**) coal and kaolinite; (**d**) coal–kaolinite system; (**e**) coal and calcite; (**f**) coal–calcite system.

In contrast, the coal–kaolinite and coal–calcite systems exhibited a transition from distinct zeta potential peaks to a single dominant peak after mixing (Figure 7c–f). The resulting peak positions differed from those of the individual components, suggesting changes in the electrokinetic characteristics of the mixed particle populations. Such changes may be associated with interparticle interactions and heteroaggregation between coal and gangue particles. Compared with quartz, kaolinite and calcite therefore showed a greater tendency to interact with coal particles, potentially facilitating slime coating. These observations are consistent with the differences in bubble-particle attachment behavior presented in Figure 6 and are further examined through DLVO calculations in the following section.

3.4. Results of DLVO Theory Calculations

To elucidate the interfacial interactions between coal and gangue minerals, the interaction energies were calculated using classical DLVO theory [23]. The calculated results are presented in Figure 8, and the corresponding zeta potentials are listed in Table 3. The natural pH values of the coal–quartz, coal–kaolinite, and coal–calcite suspensions were 7.88, 6.91, and 7.86, respectively.

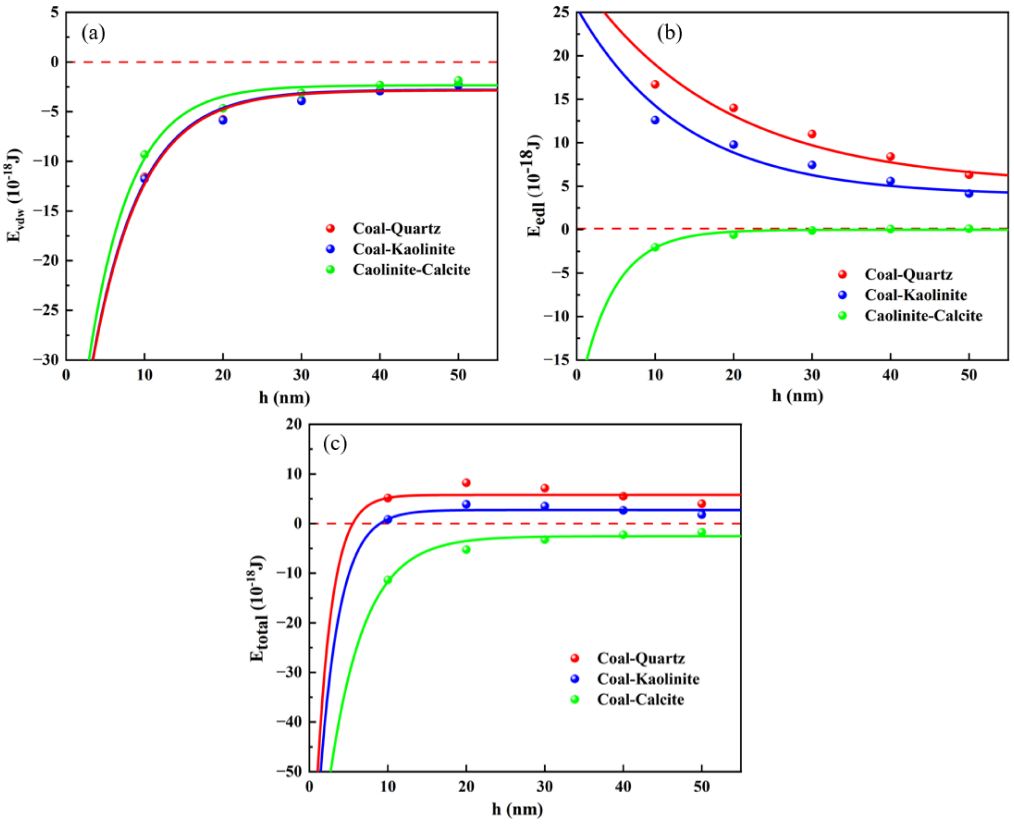


Figure 8. Interaction forces between coal and gangue minerals: (**a**) van der Waals interaction energy; (**b**) electrical double layer interaction energy; (**c**) total interaction energy.

Table 3. Zeta potentials of coal and gangue particles.

Samples	Low-Ash Coal	Quartz	Kaolinite	Calcite
Zeta potential (mV)	−20.59	−41.15	−26.42	−1.68

As shown in Figure 8a, the van der Waals interaction energies of the three coal–gangue systems were comparable and became increasingly attractive as the separation distance decreased. The differences among the systems were therefore mainly associated with the electrical double-layer interaction (Figure 8b). Owing to the strongly negative surface charges of both coal and quartz (or kaolinite), the coal–quartz and coal–kaolinite systems exhibited electrostatic repulsion. In contrast, the weakly negative surface potential of calcite greatly reduced the electrostatic barrier, allowing van der Waals attraction to become dominant at short separation distances.

Consequently, the total interaction energy (Figure 8c) remained repulsive for the coal–quartz and coal–kaolinite systems but became attractive for the coal–calcite system. Within the assumptions of classical DLVO theory, this indicates that coal–calcite heteroaggregation is energetically more favorable than that of coal–quartz and coal–kaolinite [24,41]. This baseline prediction was consistent with the zeta-potential distribution results (Figure 7), in which the coal–calcite mixture exhibited a single merged peak, supporting stronger coal–calcite association. The DLVO calculation was therefore used as a comparative mechanistic descriptor rather than as sufficient evidence of slime coating by itself.

However, the DLVO results should be regarded as a first-order interpretation of the electrostatic and van der Waals interactions rather than a complete description of the coal–gangue interface. Classical DLVO assumes relatively homogeneous particle surfaces and does not explicitly account for surface anisotropy, specific ion interactions, or chemical reactions at reactive mineral surfaces. For the coal–kaolinite system, classical DLVO predicted an overall repulsive interaction, whereas the zeta-potential distribution, SEM-EDS observations, and settling behavior indicated that kaolinite could still associate with coal surfaces. This discrepancy is consistent with the anisotropic structure of kaolinite: the basal planes are predominantly negatively charged, whereas edge charge is pH-dependent and can differ from the averaged electrokinetic response measured by zeta potential [18,42,43]. The measured zeta potential therefore may not fully represent facet-specific edge-face interactions or other short-range forces. The present data do not directly resolve the individual facet contributions, but the combined evidence indicates that classical DLVO alone is insufficient to describe the observed kaolinite association. For the coal–calcite system, the attractive DLVO prediction should also be interpreted with caution because calcite is a reactive carbonate mineral whose surface chemistry can be affected by dissolution-precipitation equilibria and aqueous Ca^{2+}/carbonate species. Thus, the present calculation represents an electrostatic-van der Waals baseline for interpreting the stronger coal–calcite association rather than a complete physicochemical model of calcite coating.

Overall, the DLVO calculations provide a useful first-order explanation for the different interaction tendencies, while the deviations observed for kaolinite and the reactive nature of calcite indicate that mineral-specific morphology and aqueous chemistry must also be considered. These limitations were therefore considered together with the zeta potential distribution, SEM-EDS, foam drainage, and settling results to interpret the contamination mechanisms.

3.5. Results of SEM-EDS Analysis

To further examine the attachment behavior of gangue minerals on coal surfaces, SEM-EDS analyses were conducted on low-ash coal and coal–gangue mixed systems. EDS spectra were collected from two representative regions of each sample to provide additional elemental information on the observed surface features. The results are presented in Figure 9.

As shown in Figure 9a, the low-ash coal exhibited a relatively smooth surface with few adhering particles. The EDS spectra were dominated by carbon, with weak Si and Al signals.

In the coal–quartz system (Figure 9b), only a few isolated particles were observed on the coal surface, with Si and O signals consistent with the presence of quartz in the binary system [15,44]. This limited attachment agreed with the strong electrostatic repulsion indicated by zeta potential measurements and DLVO calculations.

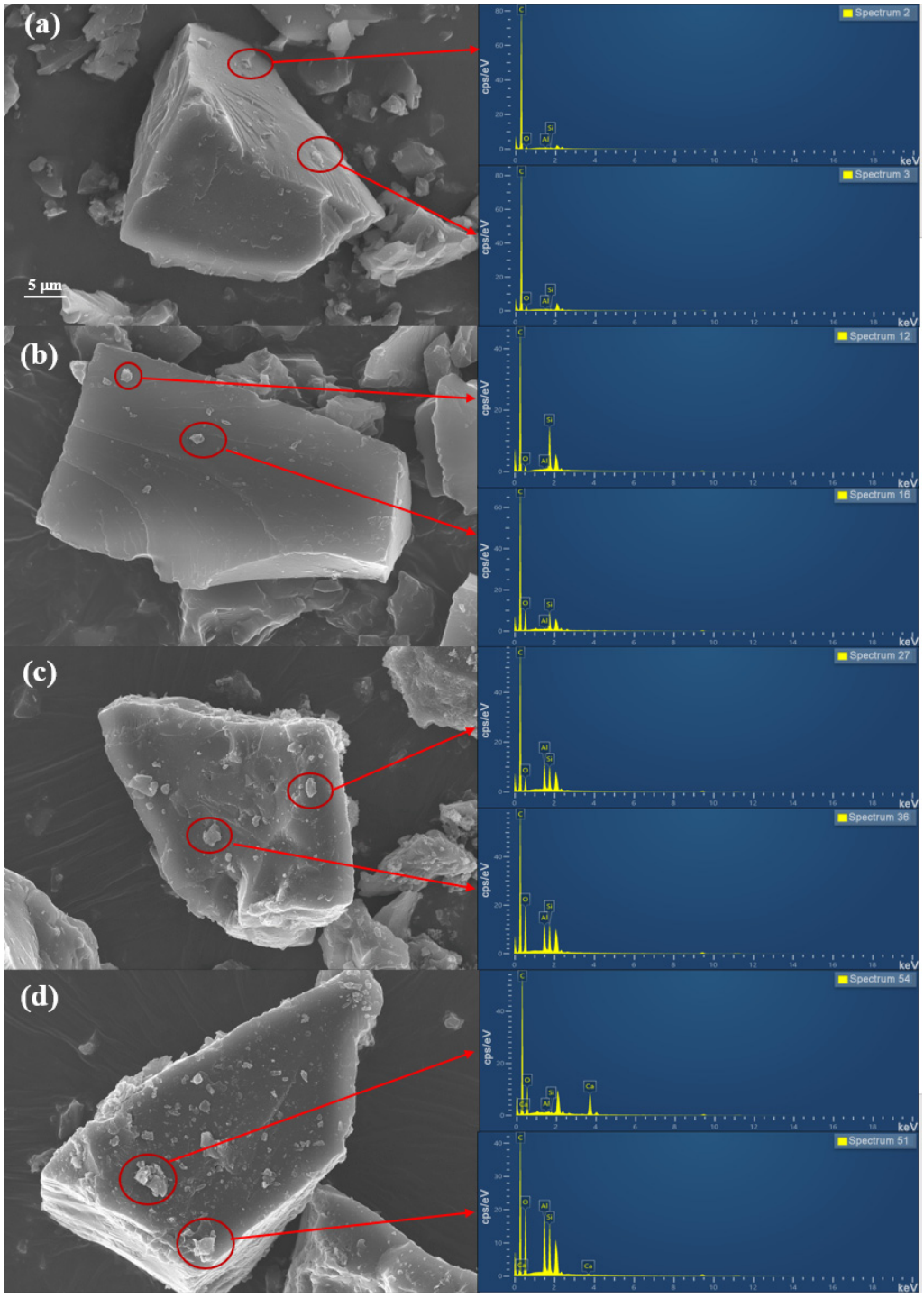


Figure 9. SEM and EDS images of coal and coal–gangue mixed systems: (**a**) coal; (**b**) coal–quartz system; (**c**) coal–kaolinite system; (**d**) coal–calcite system.

In contrast, more pronounced particle attachment was observed in the coal–kaolinite and coal–calcite systems (Figure 9c,d). The Si and Al signals supported the presence of kaolinite-associated particles, despite the repulsive interaction predicted by classical DLVO

theory, suggesting the involvement of additional mineral-specific interactions. The coal–calcite system exhibited the most pronounced particle attachment, with Ca signals providing evidence of calcite association, consistent with reduced electrostatic repulsion. The additional EDS spectra obtained from different regions further supported these observations. Overall, the qualitative attachment tendency followed the order calcite > kaolinite > quartz, consistent with the flotation results. These findings suggest that quartz contamination was more closely associated with water entrainment, whereas slime coating played a greater role in kaolinite and calcite contamination. Nevertheless, SEM-EDS provides qualitative evidence of surface association rather than a quantitative determination of the relative contributions of these contamination pathways.

3.6. Results of Foam Drainage Tests

To distinguish the contribution of water entrainment from slime coating, foam drainage tests were conducted. The results are presented in Figures 10 and 11.

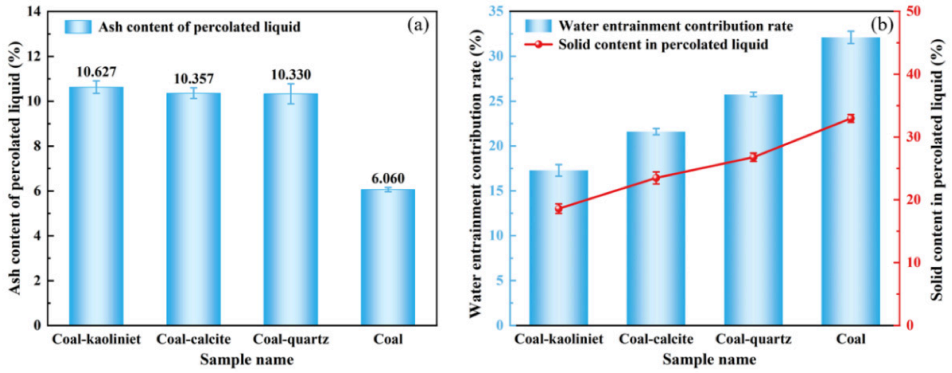


Figure 10. Foam drainage characteristics of coal–gangue systems: (**a**) contribution of water entrainment; (**b**) ash content of the drainage products.

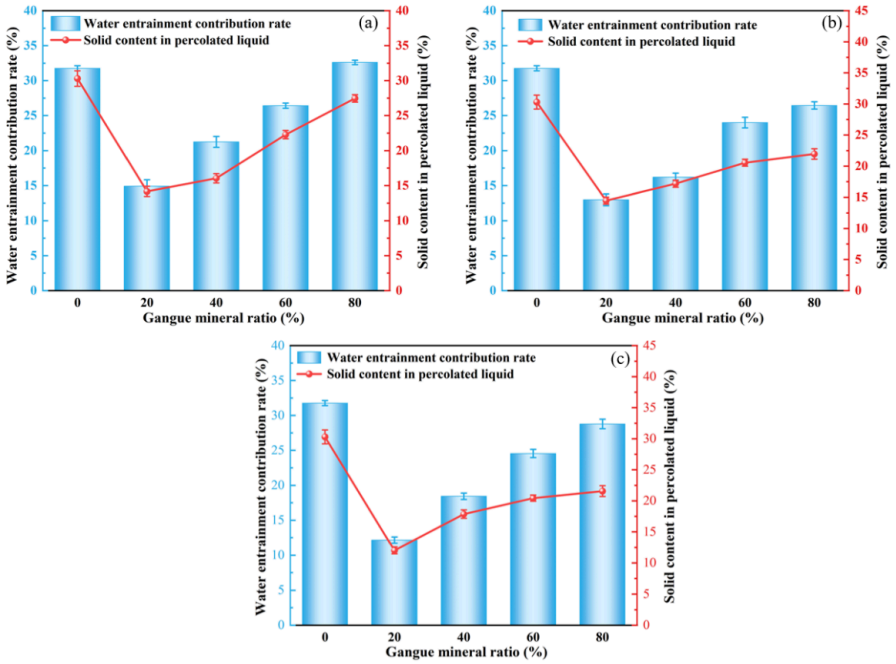


Figure 11. Foam drainage characteristics at different gangue mineral content: (**a**) coal–quartz system; (**b**) coal–kaolinite system; (**c**) coal–calcite system.

As shown in Figure 10, the contribution of water entrainment differed markedly among the three gangue minerals, following the order of coal–quartz system > coal–calcite system > coal–kaolinite system. A similar trend was observed for the solid content in the drainage products, whereas the ash content varied only slightly. Because the drainage liquid acted as the primary carrier for fine particles, the higher solid content in the coal–quartz system indicated that more gangue particles were transported by the water phase, demonstrating its stronger entrainment tendency.

Figure 11 shows the influence of gangue content on foam drainage. For all three systems, the contribution of water entrainment increased with increasing gangue content and was positively correlated with the solid content of the drainage products [15]. The substantially higher contribution in the coal–quartz system indicates a stronger tendency for fine particles to be transported through the water phase. Combined with the limited coal–quartz surface association observed by zeta potential, DLVO, SEM-EDS, and settling tests, these results support an entrainment-dominated contamination pathway for quartz [24]. In contrast, kaolinite and calcite showed stronger surface association but lower relative water-transport contributions, supporting a greater role of slime coating. The drainage results therefore provide an independent hydraulic-transport descriptor rather than a direct quantitative decomposition of total gangue recovery into entrainment and coating contributions [31].

3.7. Results of Settling Tests

To further evaluate the heteroaggregation behavior between coal and gangue minerals, settling tests were performed on pure minerals and coal–gangue mixed systems, and the results were presented in Figure 12. Results showed that the low-ash coal exhibited the slowest settling rate, whereas quartz, kaolinite, and calcite settled rapidly and formed distinct solid–liquid interfaces after 20 min. The addition of gangue minerals significantly accelerated the settling of coal suspensions. After 20 min, the clarified liquid heights followed the order of coal–calcite system (6.5 cm) > coal–kaolinite system (6.0 cm) > coal–quartz system (4.5 cm) > low-ash coal (2.2 cm), indicating that the apparent aggregation tendency followed the order of calcite > kaolinite > quartz [45].

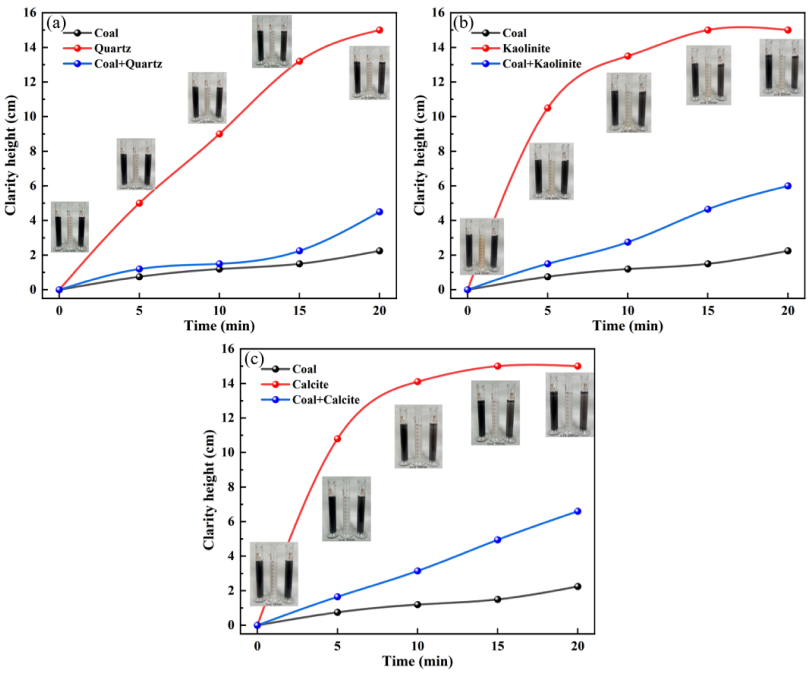


Figure 12. Settling behavior of different coal–gangue systems: (**a**) coal–quartz system; (**b**) coal–kaolinite system; (**c**) coal–calcite system.

The pronounced settling enhancement in the coal–calcite and coal–kaolinite systems indicated stronger apparent aggregation of coal–gangue particles. For the coal–calcite system, the enhanced settling was consistent with the attractive interaction predicted by the DLVO baseline. For the coal–kaolinite system, pronounced settling occurred despite the repulsive overall interaction predicted by classical DLVO, consistent with the surface association observed by SEM-EDS. This difference indicates that kaolinite aggregation under the present conditions cannot be fully described by the classical DLVO terms considered here [15,19]. In contrast, the limited settling enhancement observed for the coal–quartz system indicates comparatively weak particle association, consistent with its limited surface attachment and higher water-mediated transport during flotation [24]. The settling results therefore provide macroscopic evidence consistent with the mineral-dependent association tendencies inferred from the interfacial measurements.

4. Discussion

On the basis of this integrated evidence, the mechanism framework proposed in Figure 13 suggests that gangue contamination during coking coal flotation results from the coupled contributions of water-mediated transport and coal–gangue surface association, with their relative importance depending on the interfacial properties of the gangue minerals and the prevailing pulp chemistry. Under the investigated conditions, quartz showed weak coal–gangue association, strong electrostatic repulsion, limited surface attachment, and the highest water-transport contribution, consistent with a predominantly entrainment-controlled pathway. Calcite showed the strongest coal–gangue association and surface attachment together with a lower relative water-transport contribution, consistent with a predominantly slime-coating pathway, whereas kaolinite exhibited an intermediate and coupled behavior, with measurable surface association and aggregation despite a repulsive classical-DLVO prediction while water-mediated transport remained relevant. Within this framework, pH is an important interfacial factor because changes in pulp pH can modify the surface charge, aqueous surface chemistry, and particle–particle interactions of coal and gangue minerals, thereby potentially shifting the relative contribution of water entrainment and slime coating. This mechanistic distinction also provides a basis for process regulation: entrainment-prone gangue may be more responsive to measures controlling water recovery and froth drainage, whereas coating-prone gangue may require greater attention to dispersion, conditioning, and coal–gangue surface interactions; for minerals exhibiting coupled behavior, such as kaolinite, both aspects should be considered. This interpretation represents a mechanistic synthesis for the present model systems rather than a universal quantitative prediction for industrial mixed feeds, and further validation under different pH conditions and mixed-gangue systems is required to establish its applicability to complex industrial flotation conditions.

Although the present study provides insights into mineral-specific contamination mechanisms, the simplified binary systems do not fully represent the complexity of industrial coking coal middlings. Future research should investigate the effects of pH, reagent conditions, mineral proportions, and particle-size distributions on coal–gangue interactions and flotation selectivity. Particular attention should be given to developing targeted strategies for suppressing slime coating and reducing water entrainment. Further validation using complex industrial coal samples is also necessary to assess the practical applicability of the proposed contamination mechanisms.

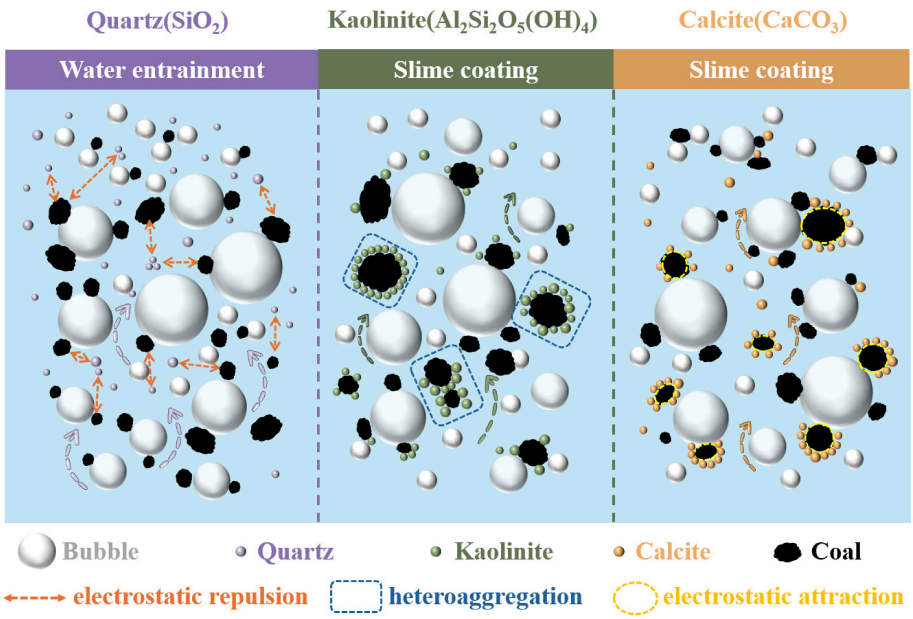


Figure 13. Proposed contamination mechanisms of gangue minerals during coking coal flotation.

5. Conclusions

This study investigated the contamination behaviors of quartz, kaolinite, and calcite in coking coal flotation through complementary experimental and theoretical analyses. The main conclusions were as follows:

(1) The addition of gangue minerals reduced combustible recovery, with the inhibitory effect following the order calcite > kaolinite > quartz. Specially, the combustible recovery decreased from 91.68% for low-ash coal to 86.87%, 84.77%, and 82.55% for the coal–quartz, coal–kaolinite, and coal–calcite systems, respectively.

(2) Quartz exhibited relatively weak coal–gangue association and a stronger tendency toward water entrainment. In contrast, calcite showed more pronounced surface attachment and aggregation, consistent with a predominantly slime-coating pathway. Kaolinite displayed intermediate behavior, with particle association that could not be fully explained by classical DLVO theory alone.

(3) Water entrainment and slime coating were interconnected contamination pathways rather than independent processes. Their relative importance depended on coal–gangue interfacial interactions, particle association, and water-mediated transport. The combined experimental evidence provided a basis for distinguishing mineral-specific contamination tendencies under controlled model-system conditions.

Author Contributions: Conceptualization, G.L. and Y.C.; methodology, L.D.; software, Y.Z., Q.Z. and L.D.; validation, J.W. and Y.Z.; formal analysis, Y.Z.; investigation, J.W. and Y.Z.; resources, G.L. and Y.C.; date curation, Y.Z. and Q.Z.; writing—original draft preparation, Y.Z.; writing—review and editing, Y.Z. and J.W.; visualization, Y.Z. and J.W.; supervision, G.L. and J.W.; funding acquisition, G.L. and Y.C. All authors have read and agreed to the published version of the manuscript.

Funding: The authors express their appreciation for the financial support from the National Key Research and Development Program of China (2023YFC2907703), the National Natural Science Foundation of China (52374281, 52204287), and the Zhongyuan Scholar Program (244000510006).

Data Availability Statement: Authors are fully responsible for the originality, validity, and integrity of the content of their manuscript.

Conflicts of Interest: The authors declare that they have no known competing financial interests or personal relationships that could have appeared to influence the work reported in this paper.

References

1. Wang, S.; Gui, D.; Kadagala, M.R.; Liao, Y. Synergistic adsorption mechanism and flotation performance of an emulsified collector derived from coal tar via kerosene extraction for coking coal: A combined experimental insight and molecular dynamics simulations. *J. Environ. Chem. Eng.* **2026**, *14*, 123372. [CrossRef]
2. Zhang, D.; Ma, X.; Dong, X.; Fan, Y.; Sun, Y.; Wen, P.; Yang, M. Interfacial modification mechanisms for enhanced flotation of hard-to-float coking coal via ultrafine grinding and SHMP/SDS synergistic conditioning. *Fuel* **2026**, *406*, 136939. [CrossRef]
3. Zhang, X.; Tao, Y. Study on dissociation characteristics and enhanced gravity separation of coking coal middlings. *Int. J. Coal Prep. Util.* **2024**, *44*, 481–502. [CrossRef]
4. Hua, Y.; Liu, W.; Zhuo, Q.; Zhang, Y. Identification and quantitative characterization of inorganic mineral embedding features in coking middling coals. *Fuel* **2026**, *404*, 136413. [CrossRef]
5. Lv, B.; Fan, W.; Jiao, Y.; Deng, X.; Xing, B. Deep recovery of clean coal from coking middlings: Pre-separation in liquid-solid fluidized bed and subsequent flotation. *Chem. Eng. Res. Des.* **2024**, *210*, 605–613. [CrossRef]
6. Xiaodong, H.; Weiran, Z.; Fengnian, S.; Wei, H. Coal middling retreatment using high voltage pulse technique. Part 1, experimental findings. *Fuel* **2022**, *314*, 123066. [CrossRef]
7. Jaiswal, S.; Singh, R.; Singh, V.; Mukherjee, A.K. A study of the effects of thermal shocks on liberation characteristics of high coal ash particles. *Fuel* **2018**, *233*, 215–223. [CrossRef]
8. Guo, K.; Zhang, D.; Guo, W.; Li, Y.; Xing, Y.; Gui, X. Impact of grinding media shape on the dissociation characteristics and flotation behavior of coking coal middlings. *Powder Technol.* **2025**, *449*, 120423. [CrossRef]
9. Wang, X.; Gao, J.; Liu, H.; Ni, C.; Zhou, S.; Xie, G.; Bu, X.; Ping, A. Mechanism of β-cyclodextrin/kerosene pickering emulsion in enhancing low-rank coal flotation. *Fuel* **2027**, *427*, 139737. [CrossRef]
10. Hua, Y.; Liu, W.; Zhuo, Q. The effect of inorganic mineral embedding features in coking middling coals on their liberation and flotation separation. *Separations* **2026**, *13*, 86. [CrossRef]
11. Kadagala, M.R.; Nikkam, S.; Tripathy, S.K. A review on flotation of coal using mixed reagent systems. *Miner. Eng.* **2021**, *173*, 107217. [CrossRef]
12. Wang, X.; Cheng, H.; Ding, D. Advances and prospects on flotation enhancement of difficult-to-float coal by emulsion: A review. *Minerals* **2024**, *14*, 952. [CrossRef]
13. Dai, M.; Zeng, H.; Tang, H.; Wang, J.; He, J.; Sun, W.; Wang, L. Suppressing fine diaspore entrainment by selective flocculation with xanthan gum in the reverse flotation desulfurization of high-sulfur bauxite. *Colloids Surf. A* **2026**, *733*, 139280. [CrossRef]
14. Wen, P.; Ma, X.; Fan, Y.; Dong, X.; Chen, R.; Chang, M.; Bai, X.; Cai, S. Insights into the interaction of polycarboxylate with coal and kaolinite and their application in flotation. *Fuel* **2023**, *340*, 127481. [CrossRef]
15. Yu, Y.; Ma, L.; Cao, M.; Liu, Q. Slime coatings in froth flotation: A review. *Miner. Eng.* **2017**, *114*, 26–36. [CrossRef]
16. Li, A.; Li, R.; Yan, C.; Wang, H.; Liu, Q.; Masliyah, J.H.; Zeng, H.; Xu, Z. The effect of clay type and solid wettability on bitumen extraction from canadian oil sands. *Fuel* **2023**, *337*, 126887. [CrossRef]
17. Yang, M.; Fan, Y.; Ma, X.; Dong, X.; Wen, P.; Xiao, W. Mechanistic study of the effects of ultrafine grinding on the surface properties of anthracite coal particles and interface regulation on froth flotation under multifactorial influences. *Fuel* **2024**, *371*, 131927. [CrossRef]
18. Li, P.; Zhang, M.; Lei, W.; Yao, W.; Fan, R. Effect of nanobubbles on the slime coating of kaolinite in coal flotation. *ACS Omega* **2020**, *5*, 24773–24779. [CrossRef]
19. Yu, Y.; Li, A.; Xu, Z.; Zhou, A.; Li, Z.; Zhang, N.; Qu, J.; Zhu, X.; Liu, Q. New insights into the slime coating caused by montmorillonite in the flotation of coal. *J. Clean. Prod.* **2020**, *242*, 118540. [CrossRef]
20. Mao, R.; Zhang, Y.; Zhu, H.; Liu, X.; Chen, J.; Min, F.; Zhu, J.; Chen, K. Study on flotation of high ash coal slime enhanced by ultrasonic threshold regulation of functional groups. *Fuel* **2026**, *409*, 137679. [CrossRef]
21. Li, J.; Zhang, Z.; Lu, H.; Zhang, W.; Xu, S.; Zhang, Y.; Deng, J.; Ma, L. Mechanism of high-intensity conditioning on the dispersion of typical slime coating in fluorite flotation. *Powder Technol.* **2026**, *469*, 121821. [CrossRef]
22. Yang, Z.; Xia, Y.; Fu, Y.; Liu, Q.; Li, M.; Gui, X. The flotation deashing separation performance of high-ash fine coal-slime using humic acid depressant and insights to its depressant mechanism. *Fuel* **2025**, *382*, 133756. [CrossRef]
23. Can, G.; Onur, G.; Mustafa, C.; Orhan, O. An investigation of the effect of clay type on coal flotation along with DLVO theoretical analyses. *Int. J. Coal Prep. Util.* **2020**, *40*, 210–222. [CrossRef]
24. Chen, Y.; Hu, S.; Li, J.; Weng, L.; Wu, C.; Liu, K. Improvement on combustible matter recovery in coal slime flotation with the addition of sodium silicate. *Colloids Surf. A* **2020**, *603*, 125220. [CrossRef]

25. Xing, Y.; Xu, M.; Guo, F.; Luo, J.; Zhang, Y.; Cao, Y.; Gui, X. Role of different types of clay in the floatability of coal: Induction time and bubble-particle attachment kinetics analysis. *Powder Technol.* **2019**, *344*, 814–818. [CrossRef]
26. Zhu, Z.; Zhao, B.; Wang, J.; Zhu, Y.; Sheng, Q.; Li, Z.; Zhang, N.; Yu, W. Reduction of slime coating: Effects of sodium silicate and sodium carbonate on lean coal flotation in sodium oleate system. *J. Dispers. Sci. Technol.* **2025**, *46*, 1205–1215. [CrossRef]
27. Li, Q.; Zhang, W.; Tan, J.; Liang, L.; Xie, G. Mechanism of slime coating on coal surface with different metamorphic degrees. *Colloids Surf. A* **2023**, *675*, 132038. [CrossRef]
28. Neethling, S.J.; Cilliers, J.J. The entrainment of gangue into a flotation froth. *Int. J. Miner. Process* **2002**, *64*, 123–134. [CrossRef]
29. Wang, L.; Peng, Y.; Runge, K.; Bradshaw, D. A review of entrainment: Mechanisms, contributing factors and modelling in flotation. *Miner. Eng.* **2015**, *70*, 77–91. [CrossRef]
30. Taner, H.A.; Onen, V. Mechanism of mechanical entrainment in chalcopyrite flotation: Effects of clay minerals. *Min. Metall. Explor.* **2024**, *41*, 311–319. [CrossRef]
31. Tan, J.; Wang, J.; Nguyen, A.V.; Xie, G. Regimes of drainage instability caused by wash water. *Miner. Eng.* **2020**, *148*, 106202. [CrossRef]
32. Wang, L.; Wang, Y.; Sun, F.; Gui, X. Revisiting the enhanced selectivity in low-rank coal flotation by composite collector comprising kerosene and sorbitan mono oleate. *Powder Technol.* **2023**, *428*, 118729. [CrossRef]
33. Wang, L.; Runge, K.; Peng, Y. The observed effect of flotation operating conditions and particle properties on water recovery at laboratory scale. *Miner. Eng.* **2016**, *94*, 83–93. [CrossRef]
34. Ducker, W.A.; Mastropietro, D. Forces between extended hydrophobic solids: Is there a long-range hydrophobic force? *Curr. Opin. Colloid Interface Sci.* **2016**, *22*, 51–58. [CrossRef]
35. Weber, C.; Knüpfer, P.; Buchmann, M.; Rudolph, M.; Peuker, U.A. A comparison between approaches for the calculation of van der waals interactions in flotation systems. *Miner. Eng.* **2021**, *167*, 106804. [CrossRef]
36. Lepage, M.R.; Visconti, L.; Opoku, J.; Waters, K.E. The role of measured froth zone water content in flotation froth stability and entrainment behaviour. *Can. Metall. Quart.* **2026**, *65*, 3198–3213. [CrossRef]
37. Ping, A.; Wu, J.; Chen, Z.; Liu, M.; Li, A.; Wei, Z.; Shi, Y.; Wang, L. Comparative study of kaolinite and montmorillonite effects on low-rank coal flotation: Focus on entrainment. *Part. Sci. Technol.* **2025**, *43*, 904–911. [CrossRef]
38. Wang, C.; Sun, C.; Liu, Q. Entrainment of gangue minerals in froth flotation: Mechanisms, models, controlling factors, and abatement techniques—A review. *Min. Metall. Explor.* **2021**, *38*, 673–692. [CrossRef]
39. Tian, Q.; Wang, H.; Pan, Y. Associations of gangue minerals in coal flotation tailing and their transportation behaviors in the flotation process. *ACS Omega* **2022**, *7*, 27542–27549. [CrossRef]
40. Yang, W.; Liu, H.; Shi, Y.; Liao, R.; Liu, H.; Wang, J. Interface mechanisms of citric acid in suppressing slime coating for enhanced separation of pyrite from sericite. *Miner. Eng.* **2026**, *243*, 110243. [CrossRef]
41. Chen, Y.; Xu, B. Insights into the flotation of cassiterite-containing clinochlore with hydrophobic entrainment based on EDLVO theory. *ACS Omega* **2025**, *10*, 28075–28082. [CrossRef]
42. Xu, Z.; Liu, J.; Choung, J.W.; Zhou, Z. Electrokinetic study of clay interactions with coal in flotation. *Int. J. Miner. Process* **2003**, *68*, 183–196. [CrossRef]
43. Lagaly, G.; Ziesmer, S. Colloid chemistry of clay minerals: The coagulation of montmorillonite dispersions. *Adv. Colloid. Interface Sci.* **2003**, *100*, 105–128. [CrossRef]
44. Ma, G.; Cui, J.; Li, J.; Bu, X.; Shao, H.; Wang, Z.; Liu, F.; Sobhy, A.; Tao, D. Nanobubble enhanced flocculation and filtration of fine coal and associated mechanisms. *Fuel* **2025**, *393*, 134989. [CrossRef]
45. Shang, H.; Chen, J.; Min, F.; Cheng, Y.; Bao, L.; Wu, Z. Microscopic interaction mechanism between Fe-doped kaolinite and quartz: DFT calculations and experiments. *Fuel* **2026**, *403*, 136074. [CrossRef]

Disclaimer/Publisher's Note: The statements, opinions and data contained in all publications are solely those of the individual author(s) and contributor(s) and not of MDPI and/or the editor(s). MDPI and/or the editor(s) disclaim responsibility for any injury to people or property resulting from any ideas, methods, instructions or products referred to in the content.